The Numerical and Experimental Investigations of a Gimballed Pendulum Energy Harvester

Trewut Anurakpandit†, Nicholas C. Townsend, and Philip A. Wilson

Fluid Structure Interactions Research Group, University of Southampton, Southampton, SO16 7QF, United Kingdom

Abstract

A simple or single-degree-of-freedom (1-DOF) pendulum system is a typical mechanism that has been used for vibration energy harvesting. Generally, a 1-DOF pendulum system is constrained to move on a single plane which limits the system when excited by multi-directional disturbances. In order to overcome this limitation, this paper considers the application of a 2-axis gimbal pendulum system. The gimballed pendulum system consists of two perpendicular horizontal pivots which allow the pendulum to achieve spherical or orbital motion around the pivots. Theoretical and experimental investigations of a gimballed pendulum energy harvesting system for multi-directional excitation are described in this paper. A mathematical model of the mechanical arrangement is derived based on the Lagrange equation and a simplified assumption that the perpendicular pivots are treated as two coupled rotating references with geometric relationships. This derived model is able to realistically reflect and identify the asymmetric properties between the coupled references created by a gimbal mechanism. The theoretical and experimental investigations of 1-DOF and coupled-DOF (2-DOF) pendulum dynamics are presented using a constant excitation amplitude over a range of frequencies with different heading angles representing the directions of the external disturbance. The numerical and experimental results show generally good correlation and the dominant coupling effect of the coupled rotating references that modulates the pendulum responses is theoretically and practically captured. Interestingly, the measured simultaneous electrical power production generated by the coupled dynamics of the gimballed pendulum achieves less power compared to when it dynamically performs as a 1-DOF system at the same disturbing condition.

Keywords: Pendulum, Gimbals, Energy harvesting, Coupled-degree-of-freedom

I. Introduction

A pendulum is a mechanical system with a mass or rigid body supported and free to swing around a pivot. By this simple arrangement, a pendulum can planarly rotate or swing around a pivot depending on the applied external excitation. Once the disturbance is taken away from the system, the pendulum will decreasingly oscillate until it rests at an equilibrium position as a result of the associated restoring force due to gravity (if it overcomes involved frictional forces). Theoretically, this mechanical system has been widely studied to represent basic vibration problems [1], [2] as well as complex non-linear [3]–[5] and chaotic behaviours [6].

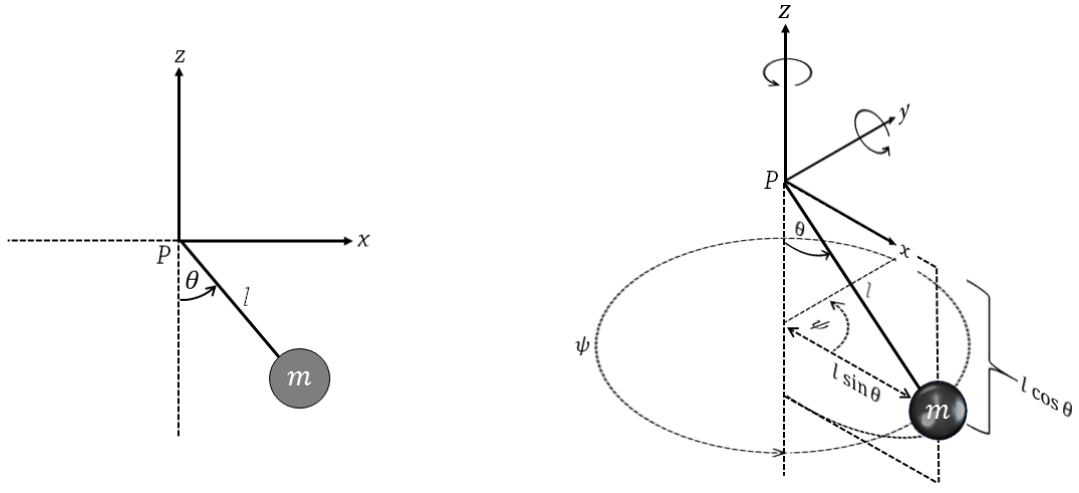

(a) Simple pendulum model.

(b) Spherical pendulum model.

Fig. 1. General pendulum theoretical models.

†Corresponding author.
E-mail addresses: T.Anurakpandit@soton.ac.uk (Trewut Anurakpandit), N.C.Townsend@soton.ac.uk (Nicholas C. Townsend).

In terms of energy harvesting, the concept of a simple or planar pendulum system has been applied to extract energy from moving machinery [7] and human movement [8], [9] and also appears in the application of wave energy conversion (WEC). For instance, the 'SEAREV' wave energy converter uses an eccentric (pendulum-like) mass which is allowed to move relatively to the floating (pitching) body [10], [11]. Also, the works in papers [12]–[14] perform theoretical studies of a pendulum electric-power generator mounted in symmetric and asymmetric floating bodies which is excited by unidirectional irregular waves. The other approach presented in several pieces of research is a parametric, vertical excited, pendulum which is designed to gain the benefit from parametric resonance from vertical excitation or heave motion of a floating platform. This type of pendulum system is theoretically and experimentally demonstrated in [15]–[18]. It should be highlighted that the mentioned designs of pendulum energy harvesters are constrained to move and allowed to be excited within a fixed plane. Thus, they can be referred as a simple or 1-DOF pendulum system, as illustrated in Figure 1(a), and mathematically expressed as:

$$ml^2\ddot{\theta}(t) + mgl\sin(\theta(t)) = Q_\theta \tag{1}$$

where m is weight of pendulum mass (kg), l is length of the pivot to centre of gravity (CG) of pendulum or pendulum arm (m), ml^2 represents mass moment of inertia (kg·m^2), g is gravity acceleration (m/s^2), θ is angular displacement (rad) referenced to the vertical axis (z-axis), and Q_θ represents generalised torque and damping component(s), i.e., power-take-off (PTO) and frictional torques at the pivot [2], [19]. A derivation of the equation of motion of an externally excited simple pendulum system is given in Appendix A.

In general, environment excitation is not always unidirectional e.g. ocean waves. As a result, 1-DOF pendulum systems constrained within a fixed plane, may be limited. To overcome this, a 2-axis gimballed pendulum energy harvesting system, with perpendicular horizontal pivots that allows spherical or orbital pendulum rotations, such as the proposed WITT (Whatever Input to Torque Transfer) device introduced by [20] is a prototype of a gimballed pendulum energy harvesting device designed for harvesting vibration energy from random directional disturbance condition. This device is able to transfer its spherical pendulum rotation into unidirectional output via a gearbox mechanism connected at the pivots. However, the theoretical and experimental investigations of using the WITT device to harvest ocean wave energy treat and analyse the system as a 1-DOF pendulum [21]. That is, the dynamics a multiple- or coupled-DOF pendulum energy conversion system remains uninvestigated. Yet, in theory, the dynamics of spherical-path pendulum in three-dimensional (3-D) domain is normally referred to as a spherical or conical pendulum model as shown in Figure 1(b) that can be mathematically expressed as 2-DOF dynamics system as:

$$ml^2\ddot{\theta}(t) + mgl\sin(\theta(t)) - ml^2\sin(\theta(t))\cos(\theta(t))\dot{\psi}(t)^2 = Q_\theta, \tag{2}$$

$$ml^2\sin(\theta(t))^2\ddot{\psi}(t) = Q_\psi \tag{3}$$

where the parameters (m, l, and g) of this spherical pendulum model are similar to the simple pendulum system in Equation 1 which are defined regarding two generalised coordinates; θ and ψ are the DOFs of the angular position respecting the vertical axis (z-axis) and the angular position on the horizontal plane (xy-plane) referenced to x-axis or the azimuth angle with the generalised torques, Q_θ and Q_ψ, respectively [22], [23]. A derivation of the equation of motion of an externally excited spherical pendulum system is given in Appendix B.

However, the spherical pendulum model, Equations 2 and 3, is unable to theoretically explain the dynamics of a gimballed pendulum with external excitation. Due to, first, the rotating definition made in the spherical pendulum model not representing the rotating arrangement provided by a pendulum with 2-axis gimballed pivots. Second, a gimbal mechanism creates asymmetric inertial properties of two perpendicular pivots but a symmetric inertia is only suggested by the existing model. Therefore, to theoretically model a gimballed pendulum system and to investigate and understand its coupled dynamics are major challenges.

This paper proposes a theoretical approach based on Lagrange equation to formulate the equations of motion of a gimballed pendulum system. The coupled-DOF dynamics of the two perpendicular pendulum rotating references is mathematically and experimentally investigated. The novel comparison of 1- and coupled-DOFs dynamic responses are detailed. Also, for energy conversion application, the power generation performances of the investigated pendulum systems are demonstrated.

This paper is organised as follows: Section II details the formulation of the equations of motion of a gimballed pendulum model based on a coupled 2-DOF dynamics model respecting two perpendicular horizontal pendulum pivots. Next, the design of a gimballed pendulum energy harvester prototype and the detail of the experimental validations are presented in Section III. Then, the numerical and experimental results are compared, analysed, and discussed in Section IV. Lastly, Section V summarises the key findings discovered in this research.

II. Methodology

A. Working Principle and the Equations of Motion

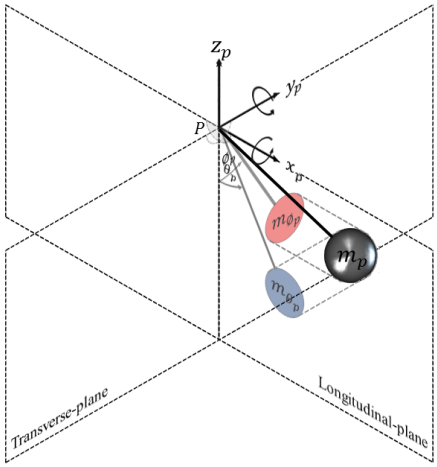

(a) Schematic diagram of the whole system.

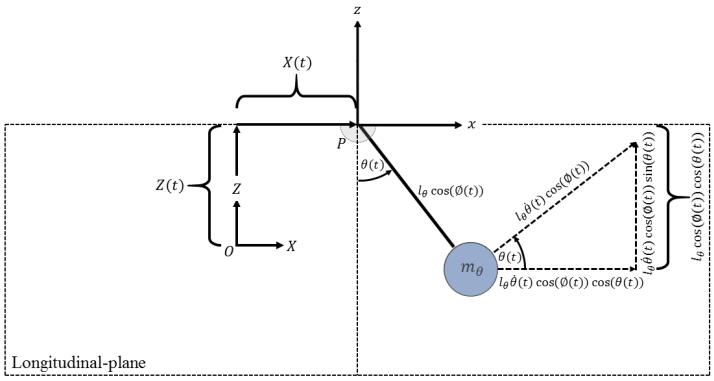

(b) Longitudinal-plane (θ-plane) pendulum reference.

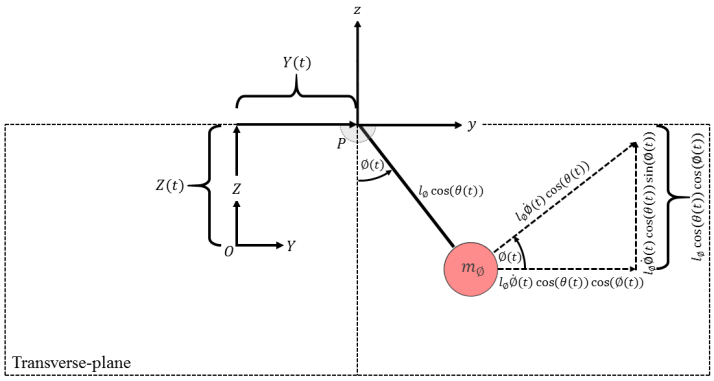

(c) Transverse-plane (ϕ-plane) pendulum references.

Fig. 2. Schematic diagram of simplified rotating references of a gimballed pendulum system.

To model the system, the pendulum system in Figure 2(a) is simplified and divided into two coupled planar pendulum systems which are 'longitudinal-plane' and 'transverse-plane' given as θ- and ϕ-planes pendulum systems respectively as illustrated in Figures 2(b) and 2(c). Each pendulum system consists of a mass (m_θ or m_ϕ) supported at a pivot from a distance away from the CG (l_θ or l_ϕ). So, there are two generalised coordinates, θ and ϕ, defined for these coupled pendulum systems. Once the axial excitations along x-, y-, and z-axes are applied, the pivoted point (P) is moved away from the initial position representing global coordinate $PXYZ$; PXZ for θ-plane reference and PYZ for ϕ-plane reference. As both pendulum dynamics are coupled with the cosine functions, $\cos(\theta(t))$ and $\cos(\phi(t))$, the kinetic and potential energies for the θ-plane pendulum can therefore be calculated as:

$$\begin{aligned}
T_\theta(t) &= \frac{1}{2} m_\theta v_\theta(t)^2 \\
&= \frac{1}{2} m_\theta \Big(\mathbf{v}_x(t) + \mathbf{v}_z(t) \Big)^2 \\
&= \frac{1}{2} m_\theta \Big(\big(\dot{X}(t) + l_\theta \dot{\theta}(t) \cos(\phi(t)) \cos(\theta(t)) \big) + \big(\dot{Z}(t) + l_\theta \dot{\theta}(t) \cos(\phi(t)) \sin(\theta(t)) \big) \Big)^2 \\
&= \frac{1}{2} m_\theta \Big(\dot{X}(t) + \dot{Z}(t) + l_\theta^2 \dot{\theta}(t)^2 \cos(\phi(t))^2 + 2 l_\theta \dot{\theta}(t) \cos(\phi(t)) \big(\dot{X}(t) \cos(\theta(t)) + \dot{Z}(t) \sin(\theta(t)) \big) \Big),
\end{aligned} \tag{4}$$

and

$$\begin{aligned}
V_\theta(t) &= m_\theta g h_\theta(t) \\
&= m_\theta g Z(t) + m_\theta g l_\theta \cos(\phi(t)) \Big(1 - \cos(\theta(t)) \Big),
\end{aligned} \tag{5}$$

and, therefore, the Lagrangian ($L_i = T_i - V_i$) of the longitudinal reference (L_θ) is

$$\begin{aligned}
L_\theta(t) = \frac{1}{2} m_\theta \Big(\dot{X}(t) + \dot{Z}(t) + l_\theta^2 \dot{\theta}(t)^2 \cos(\phi(t))^2 + 2 l_\theta \dot{\theta}(t) \cos(\phi(t)) \big(\dot{X}(t) \cos(\theta(t)) + \dot{Z}(t) \sin(\theta(t)) \big) \Big) \\
- m_\theta g Z(t) + m_\theta g l_\theta \cos(\phi(t)) \Big(1 - \cos(\theta(t)) \Big)
\end{aligned} \tag{6}$$

Likewise, for the ϕ-plane pendulum, as:

$$\begin{aligned}
T_\phi(t) &= \frac{1}{2} m_\phi v_\phi(t)^2 \\
&= \frac{1}{2} m_\phi \Big(\mathbf{v}_y(t) + \mathbf{v}_z(t) \Big)^2 \\
&= \frac{1}{2} m_\phi \Big(\big(\dot{Y}(t) + l_\phi \dot{\phi}(t) \cos(\theta(t)) \cos(\phi(t)) \big) + \big(\dot{Z}(t) + l_\phi \dot{\phi}(t) \cos(\theta(t)) \sin(\phi(t)) \big) \Big)^2 \\
&= \frac{1}{2} m_\phi \Big(\dot{Y}(t) + \dot{Z}(t) + l_\phi^2 \dot{\phi}(t)^2 \cos(\theta(t))^2 + 2 l_\phi \dot{\phi}(t) \cos(\theta(t)) \big(\dot{Y}(t) \cos(\phi(t)) + \dot{Z}(t) \sin(\phi(t)) \big) \Big),
\end{aligned} \tag{7}$$

and

$$\begin{aligned}
V_\phi(t) &= m_\phi g h_\phi(t) \\
&= m_\phi g Z(t) + m_\phi g l_\phi \cos(\theta(t)) \Big(1 - \cos(\phi(t)) \Big).
\end{aligned} \tag{8}$$

and, therefore, the Lagrangian of the transverse reference (L_ϕ) is

$$\begin{aligned}
L_\phi(t) = \frac{1}{2} m_\phi \Big(\dot{Y}(t) + \dot{Z}(t) + l_\phi^2 \dot{\phi}(t)^2 \cos(\theta(t))^2 + 2 l_\phi \dot{\phi}(t) \cos(\theta(t)) \big(\dot{Y}(t) \cos(\phi(t)) + \dot{Z}(t) \sin(\phi(t)) \big) \Big) \\
- m_\phi g Z(t) + m_\phi g l_\phi \cos(\theta(t)) \Big(1 - \cos(\phi(t)) \Big).
\end{aligned} \tag{9}$$

From the Lagrange equation, the governing equations in the generalised coordinates for this pendulum system are

$$\frac{d}{dt} \left(\frac{\partial L_\theta}{\partial \dot{\theta}} \right) - \frac{\partial L_\theta}{\partial \theta} = Q_\theta \quad \text{and} \quad \frac{d}{dt} \left(\frac{\partial L_\phi}{\partial \dot{\phi}} \right) - \frac{\partial L_\phi}{\partial \phi} = Q_\phi. \tag{10}$$

Finally, the general equations of motion of this gimballed pendulum system can be formulated as:

$$\ddot{\theta}(t)+\frac{m_\theta g l_\theta}{I_\theta\cos(\phi(t))}\sin(\theta(t))-\dot{\phi}(t)\sin(\phi(t))\Big(\frac{2\dot{\theta}(t)}{\cos(\phi(t))}+\frac{m_\theta l_\theta}{I_\theta\cos(\phi(t))^2}\big(\dot{X}(t)\cos(\theta(t))+\dot{Z}(t)\sin(\theta(t))\big)\Big)$$
$$+\frac{m_\theta l_\theta}{I_\theta\cos(\phi(t))}\Big(\ddot{X}(t)\cos(\theta(t))+\ddot{Z}(t)\sin(\theta(t))\Big)=\frac{Q_\theta}{I_\theta\cos(\phi(t))^2}, \tag{11}$$

$$\ddot{\phi}(t)+\frac{m_\phi g l_\phi}{I_\phi\cos(\theta(t))}\sin(\phi(t))-\dot{\theta}(t)\sin(\theta(t))\Big(\frac{2\dot{\phi}(t)}{\cos(\theta(t))}+\frac{m_\phi l_\phi}{I_\phi\cos(\theta(t))^2}\big(\dot{Y}(t)\cos(\phi(t))+\dot{Z}(t)\sin(\phi(t))\big)\Big)$$
$$+\frac{m_\phi l_\phi}{I_\phi\cos(\theta(t))}\Big(\ddot{Y}(t)\cos(\phi(t))+\ddot{Z}(t)\sin(\phi(t))\Big)=\frac{Q_\phi}{I_\phi\cos(\theta(t))^2} \tag{12}$$

where $\dot{X}$, $\dot{Y}$, $\dot{Z}$, $\ddot{X}$, $\ddot{Y}$, and $\ddot{Z}$ are the first and second time-derivatives of the excitations along the local x-, y-, and z-axes respectively and I_θ and I_ϕ are mass moments of inertia of the pendulum systems. The frictional damping terms (Q_θ and Q_ϕ) can be represented as:

$$Q_\theta=-\tau_\theta\,\mathrm{sgn}(\dot{\theta}(t)), \tag{13}$$
$$Q_\phi=-\tau_\phi\,\mathrm{sgn}(\dot{\phi}(t)) \tag{14}$$

where τ_θ and τ_ϕ are frictional torques (kg·m^2) respecting the generalised coordinates. Then for 1-DOF pendulum dynamics investigation, the equation of motion of the pendulum system can be expressed as:

$$\ddot{\theta}(t)+\frac{m_\theta\, g l_\theta}{I_\theta}\sin(\theta(t))+\frac{m_\theta\, l_\theta}{I_\theta}\Big(\ddot{X}(t)\cos(\theta(t))+\ddot{Z}(t)\,\sin(\theta(t))\Big)=Q_\theta\quad\text{for }\theta\text{-plane} \tag{15}$$

or

$$\ddot{\phi}(t)+\frac{m_\phi g l_\phi}{I_\phi}\sin(\phi(t))+\frac{m_\phi l_\phi}{I_\phi}\Big(\ddot{Y}(t)\cos(\phi(t))+\ddot{Z}(t)\sin(\phi(t))\Big)=Q_\phi\quad\text{for }\phi\text{-plane.} \tag{16}$$

as the uncoupled primary resonances for each rotating references can be approximated using linear approximation detailed in Equation 31 in Appendix A.

The equations of motion of both 1-DOF (Equations 15 and 16) and 2-DOF (Equations 11 and 12) pendulum dynamics were numerically solved using 4$^{\text{th}}$-order Runge-Kutta (RK4) integration method with time step (Δt) of 0.001 second.

III. Experimental Set-up

A. Experimental Arrangement

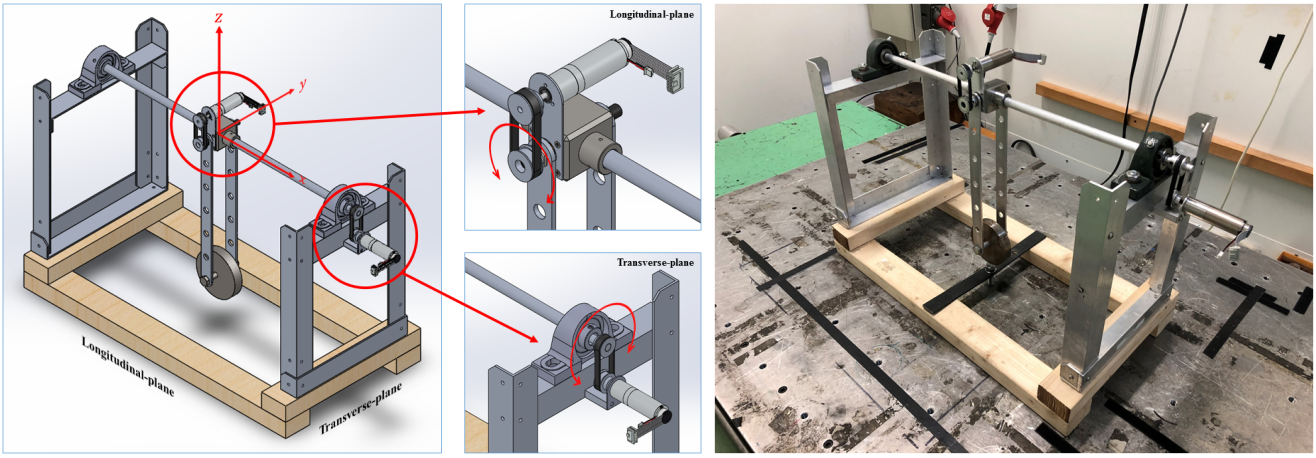

(a) 3-D Graphical design.

(b) Actual manufactured design on the test rig.

Fig. 3. Design of the investigated pendulum system.

A prototype of a gimballed pendulum energy harvester was experimentally investigated to validate the result for the pendulum response prediction described in Section II and to provide more understanding of the coupled dynamics of the pendulum system. Figure 3 shows the designed gimballed pendulum system which comprises of a metal hub with a long shaft through the middle. The hub is connected to two sets of perpendicular bearings creating two horizontal axes gimballed pivots with a disk-shape mass attached to two aluminium arms. At the pivots, rotary potentiometers (angular motion sensors) or electric generators (PTO units with encoders) were attached and driven directly through the rubber belts which are directly driven by the attached 1:1 ratio pulley wheels and, moreover, each pivot can also be constrained or locked for 1-DOF dynamics investigation. This pendulum unit is supported by two rigid aluminium frames at the both ends.

A series of experiments were conducted in the Human Factors Research Unit (HFRU) laboratory of the University of Southampton, UK [24]. The pendulum prototype was attached to a horizontal motion simulator that is capable of generating single-axis harmonic motion. The pendulum angular motions were measured by rotary potentiometers for non-PTOs cases and by digital encoders attached to the DC generators for applied PTOs conditions. The two MAXON DCX22L-EB-KL-12V DC motors acting as generators with 1:44 planetary gearhead were used as PTO units. For the power generation measurement, the electrical powers generated by the two pendulum references were calculated using Ohm's law based on the measured voltages across a constant load resistance. All the measured data were acquired using a National Instruments' NI cRIO-9022 unit and the LabVIEW software package with a sampling rate of 100 Hz.

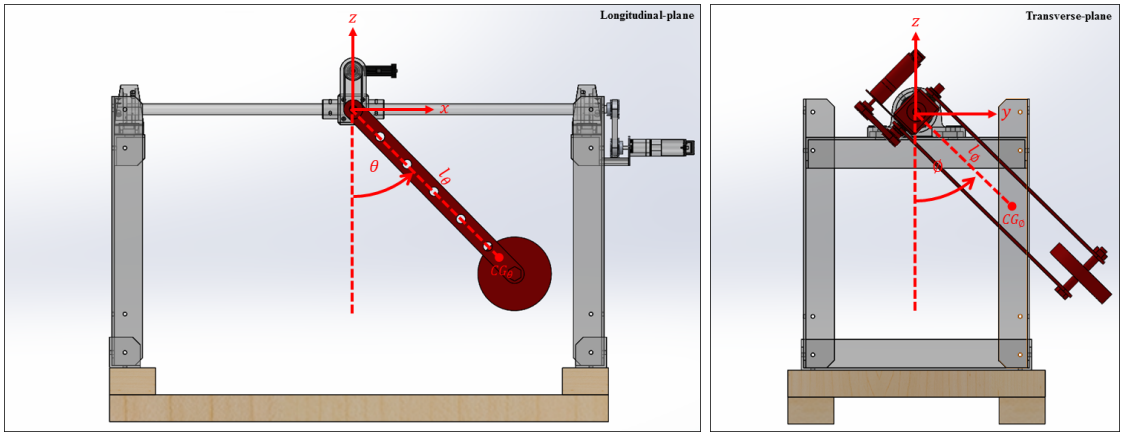

(a) θ-plane pendulum. (b) ϕ-plane pendulum.

Fig. 4. Pendulum rotating references (movable parts respecting to the rotating references are highlighted in red).

The physical parameters such as the individual pendulum weights, pivot-to-CG pendulum lengths, mass moments of inertia, and also damping constants are calculated based on the experimental measurements respecting the two pendulum rotating references as presented in Figures 4(a) and 4(b) without and with installed PTO units, the DC generators with encoders. The asymmetric inertial properties of two pendulum references are summarised in Table I.

TABLE I
THE PARAMETERS OF THE GIMBALLED PENDULUM SYSTEM

Pendulum Reference	Parameter	Symbol	Value		Unit
			without Applied PTO	with Applied PTO	
θ-plane	Pendulum Mass	m_θ	1.23934	1.23934	kg
	Pendulum Pivot-to-CG Length	l_θ	0.27801	0.27801	m
	Pendulum Mass Moment of Inertia	I_θ	0.10245	0.10249	kg·m^2
	Undamped Primary Resonance (Uncoupled)	$\omega_{n,\theta}$	0.91416	0.91399	Hz
	Damping/Frictional Torque	τ_θ	0.01743	0.02779	N·m
ϕ-plane	Pendulum Mass	m_ϕ	2.23593	2.24356	kg
	Pendulum Pivot-to-CG Length	l_ϕ	0.15347	0.15278	m
	Pendulum Mass Moment of Inertia	I_ϕ	0.10248	0.10254	kg·m^2
	Undamped Primary Resonance (Uncoupled)	$\omega_{n,\phi}$	0.91217	0.91140	Hz
	Damping/Frictional Torque	τ_ϕ	0.02561	0.05623	N·m

B. Investigated Conditions

TABLE II
TEST CONDITIONS MATRIX AT $X_\circ$ = 0.01 M

Damping Condition	Case No.	Pendulum Reference		Dynamics Type
		θ-plane	ϕ-plane	
without Applied PTOs	A1	Free	Locked	**1-DOF**
	A2	Locked	Free	
	A3	Free	Free	**2-DOF**
with Applied PTOs	B1	Free	Locked	**1-DOF**
	B2	Locked	Free	
	B3	Free	Free	**2-DOF**

[a] Ω = 0.7, 0.8, 0.9, 0.95, 1.0, 1.1, 1.2, 1.3 Hz
[b] μ = 0°, 15°, 30° 45°, 60°, 75°, 90°

The pendulum prototype was investigated as summarised in the test matrix in Table II. The 1-DOF dynamics regarding two pendulum rotating references were experimentally tested as the pendulum was constrained to swing on a particular reference and another as no rotation was allowed about the constrained axis. For the 2-DOF cases, the pendulum prototype was tested based on that both of the pivots were fully unlocked. The tests were numerically and experimentally run across a range of base excitation frequencies[a] (Ω) with a constant amplitude ($X_\circ$ = 0.01 m) and a set of heading angle[b] (μ).

A horizontal harmonic motion with a constant amplitude ($X_\circ$) is produced by the motion simulator. Therefore, the time-dependant position (X_B) of the base excitation without applied heading angle (μ) is

$$X_B(t) = X_\circ \sin(\Omega t) \tag{17}$$

and, therefore, the axial positions of the pendulum pivot(s) on global coordinate ($PXYZ$) with applied heading angle can be expressed as:

$$X(t) = X_B(t)\cos(\mu) = X_\circ \sin(\Omega t)\cos(\mu), \tag{18}$$

$$Y(t) = X_B(t)\sin(\mu) = X_\circ \sin(\Omega t)\sin(\mu), \tag{19}$$

$$Z(t) = 0. \tag{20}$$

IV. RESULTS AND DISCUSSION

A. Pendulum Responses

The RMS values of the constrained or 1-DOF pendulum responses without and with applied PTOs over the investigated frequency range and heading angles (μ) are presented in Figures 5(a), 5(b), 7(a) and 7(b). The overall comparisons of the numerical predictions and experimental results of the frequency dependant 1-DOF responses show qualitatively and quantitatively good agreement. The greatest motions emerge around the approximated primary resonance of 0.9 Hz as expected for both rotating references which are demonstrated in the time domain responses in Figures 6(a), 6(b), 8(a) and 8(b). These 1-DOF dynamics also occur in the unconstrained pendulum as case A3 and B3 at μ = 0° and 90°. This is because of the simplified 2-DOF mathematical pendulum model, Equations 11 and 12, and the experiment can be identified due to the pendulum ideally behave as a simple or 1-DOF pendulum system. This generally good correlation between the simplified 2-DOF pendulum model and the gimballed pendulum system experiments provides the confidence that the formed theoretical model is able to establish reasonable predictions when the excitation is parallel to a horizontal axis (x- or y-axes) is applied. In other words, for μ = 0° and 90°, the pendulum system behaves as a simple pendulum system as the coupling relationships/terms in the equations of motion, Equations 11 and 12, are small.

The responded motion amplitudes both numerical simulations and experimental investigations in all conducted tests are lower when the PTO units are applied since the damping values for both rotating references are greater. When the excitation is not parallel to the referenced horizontal axes (x- and y-axes), the excitations along the both axes are contributed due to the mathematical relationships in Equations 18 and 19. The θ-plane pendulum responses decrease as $\mu > 0°$, disappearing when $\mu = 90°$. Similarly, the ϕ-plane pendulum dynamically behaves in the opposite aspect.

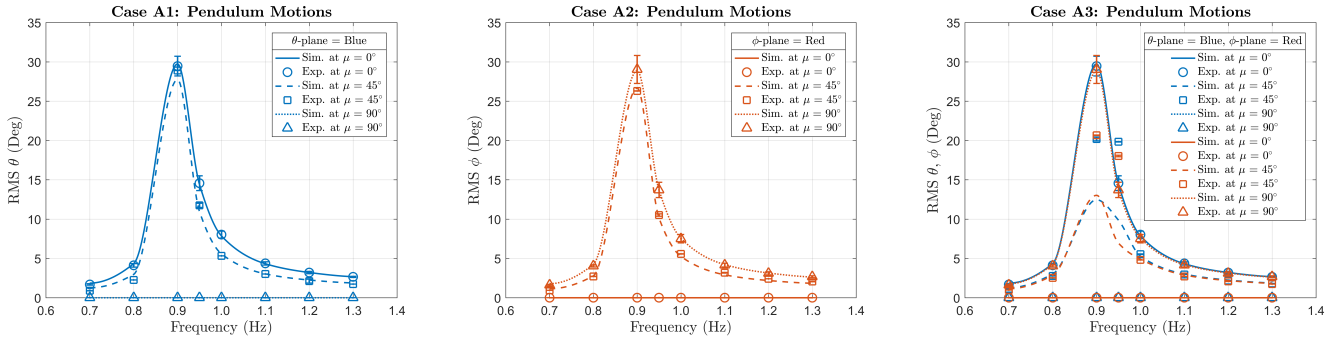

(a) Case A1. (b) Case A2. (c) Case A3.

Fig. 5. The RMS at the last 30 seconds of the pendulum responses without PTOs in frequency domain.

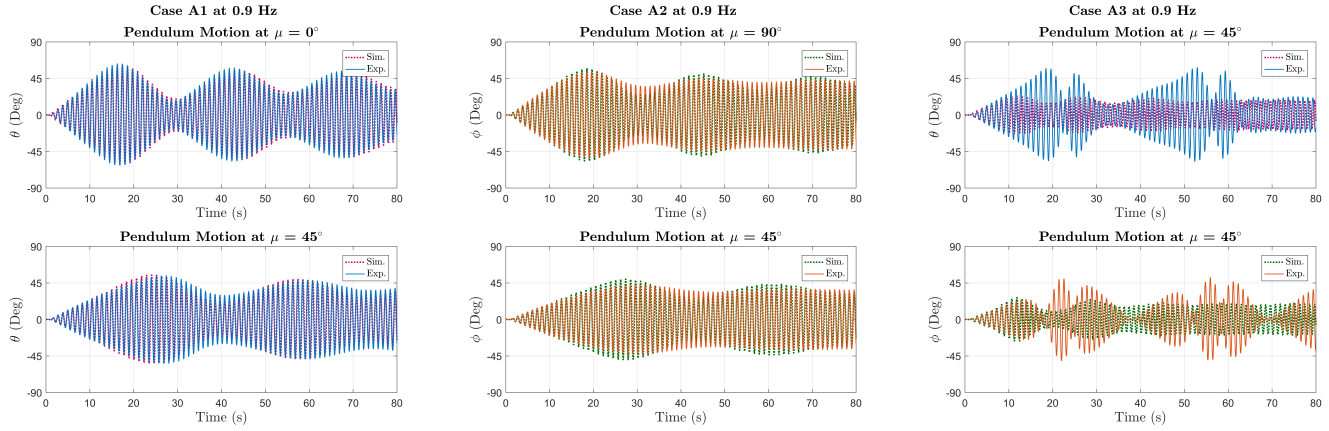

(a) Case A1. (b) Case A2. (c) Case A3.

Fig. 6. The time history pendulum responses without PTOs at Ω = 0.9 Hz.

Generally, the responded motion amplitudes of the θ-plane pendulum reference appear to be greater than the ϕ-plane pendulum in all tested circumstances. This is because of the combined perpendicular pivots created by the gimbal mechanism leads to non-equivalent mass distributions between the dynamic references, see Figure 4. For this case, the θ-plane pendulum comprises less mass, mass moment of inertia, and the parameters-related frictional torque as detailed in Table I. Therefore, it may be possible to design or tune the system to have different primary resonances between the reference planes which may be particularly useful for asymmetric systems e.g. marine vessels.

The non-linearity of the exhibited motions from both the theoretical prediction and experiment can be observed during the test period. The recorded motions, may, not finally reach steady-state responses. Thereby, a longer test duration is potentially required in order to cover all the characteristics of the oscillation response. Moreover, the small differences between the numerical and experimental results at the estimated resonance with applied PTO, especially for the phi -plane pendulum reference in Figure 8(b), are attributed to slight discrepencies in the estimated frictional damping constants, τ_θ and τ_ϕ.

For the fully coupled pendulum dynamics without applied PTO units, case A3 at μ = 45°, the good agreements of the coupled dynamic pendulum responses between numerical and experimental results are found outside the estimated resonance region with comparable responded amplitudes to the planar responses as, case A1 and A2, at similar excitation frequencies. However, around resonance, significant differences in the numerical predictions and experimental results are clearly observed. The observation shows that the responded motions of the two rotating references are distinctively lower comparing to when it performed as a simple pendulum due to the duplicate disturbances due to the coupling effect between two dynamic references. The responded characteristics and magnitudes of either pendulum references predicted by the 2-DOF gimballed pendulum numerical model appear to be different from the results obtained by the experiment.

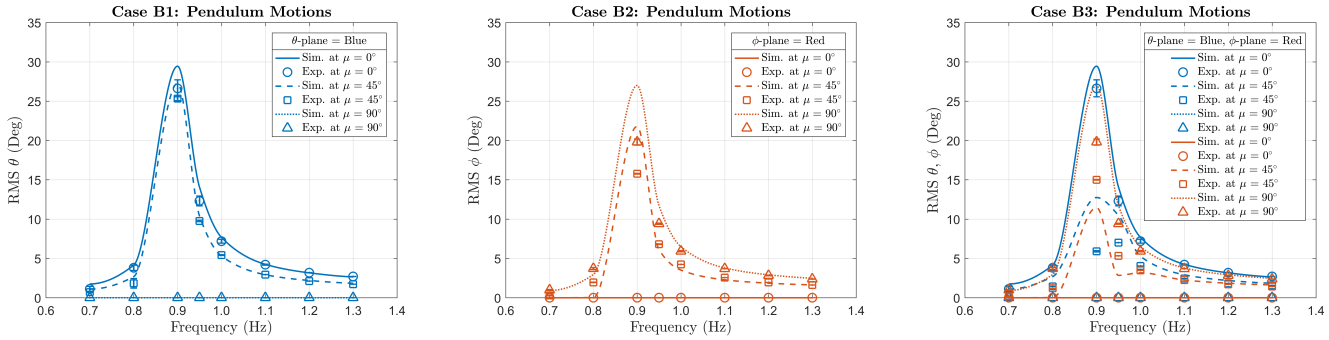

(a) Case B1. (b) Case B2. (c) Case B3.

Fig. 7. The RMS at the last 30 seconds of the pendulum responses with PTOs in frequency domain.

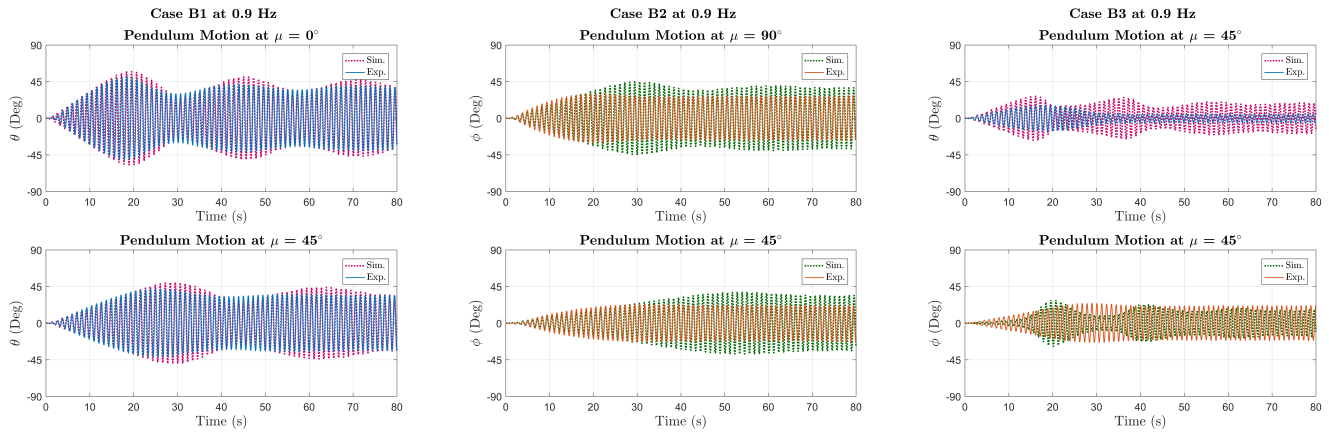

(a) Case B1. (b) Case B2. (c) Case B3.

Fig. 8. The time history pendulum responses with PTOs at Ω = 0.9 Hz.

Further, when the PTO units are applied in case B3, a similar response to case A3 with the modulated responses. Outside resonance, the coupled pendulum motion amplitudes are comparable to the 1-DOF responses is observed. Therefore, these theoretically and experimentally imply that the coupling effect between two pendulum references at the non-resonant regions is insignificant and potentially neglectable when the responded motion amplitudes are small. At and around the estimated resonance, the mathematical model captures the expected trends and tentatively indicates the effect of the coupling phenomena that modulates both pendulum motions moving with respect to the two referenced pivots, although, compared to the experiments the amplitudes differ. Therefore, it can be concluded that the mathematical model is unable to reflect all the characteristic aspects of the real physics of a gimballed pendulum system. This is due to the fact that the assumption made in the numerical modelling simplified the dynamics of this type of pendulum with applied disturbance regarding only the dynamics of two inertial perpendicular reference planes which are the DOFs moving around two horizontal axes (x- and y-axes) or generalised coordinates (θ and ϕ). Hence, the dynamic definition around the vertical axis (z-axis) is required to fulfil the physics of this pendulum system. Nonetheless, with the potential asymmetric physical property of the pendulum using gimballed pivots, the determination of the equations of motion which include all DOFs is theoretically more complex and not straightforward.

B. Measured Power Generations

In terms of the power generation, the maximum power generated by both 1-DOF and gimballed pendulum systems was experimentally measured around the linear resonance frequency (0.9 Hz) for all heading angles (μ) as plotted in Figures 9 and 10. For the direction of the applied excitation parallel to a horizontal axis (x- or y-axis) or μ = 0° and 90°, the comparisons of the 1-DOF dynamics power productions (case B1 and B2) at these heading angles between two pendulum references, θ- and ϕ-planes, show that the θ-plane pendulum achieves higher power magnitude (both in peak amplitude and RMS) that corresponds to the greater responded motion amplitude which provides larger angular velocity to drive the DC generator. The power generations of both rotating references reduce with the increasing relative heading angles acting on the horizontal axes (x- and y-axes) as illustrated in Figures 9(a) and 9(b).

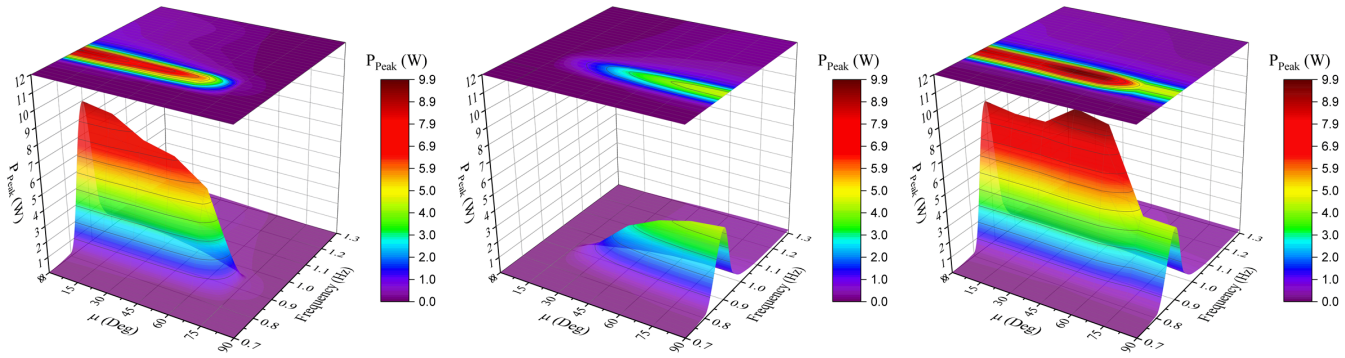

(a) Case B1 - θ-plane power. (b) Case B2 - ϕ-plane power. (c) Case B1 + Case B2 power (example case).

Fig. 9. The measured steady-state peak powers of the 1-DOF pendulum responses.

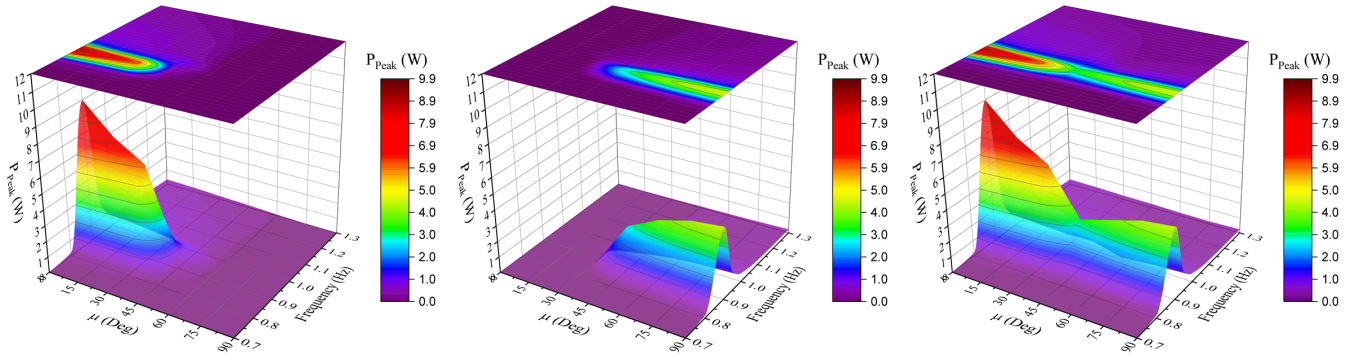

(a) Case B3 - θ-plane power. (b) Case B3 - ϕ-plane power. (c) Case B3 - total power.

Fig. 10. The measured steady-state peak powers of the coupled-DOF pendulum responses.

For case B3, at μ = 0° and 90°, both rotating references generate the same power as a 1-DOF pendulum. At applied heading angles (0° < μ < 90°), the coupled motions are able to simultaneously generate power. Figures 10(a) and 10(b) exhibit the power productions by the coupled rotating references in different heading angles which can be summed up into total generated power shown in Figure 10(c). However, the overall comparisons between 1- and coupled-DOFs over the applied excited frequencies and heading angles for the individual pendulum references clearly show that the coupled motions of the gimballed pendulum generate less power. This is due to the dominant coupling effect between the two pendulum dynamics resulting in the modulated motion amplitudes and angular velocities.

Overall, it may be stated that the gimbal mechanism is able to add compactness in design and directional responsiveness to a pendulum energy harvesting system. The maximum individual power generation level of each rotating reference could be achieved where the direction of applied excitation is parallel to a horizontal referenced axis (x- or y-axis) or, in this case, at μ = 0° and 90°. In other words, the pendulum identically responds as a 1-DOF system. Nevertheless, when the excitation is not parallelly applied to a particular horizontal axis, the coupled pendulum dynamics create undesired effect that results in a lower response compared to when it performs as a planar or 1-DOF pendulum. This leads to the lower power generations at oblique heading angles (0° < μ < 90°) as illustrated in Figures 11(a) and 11(b).

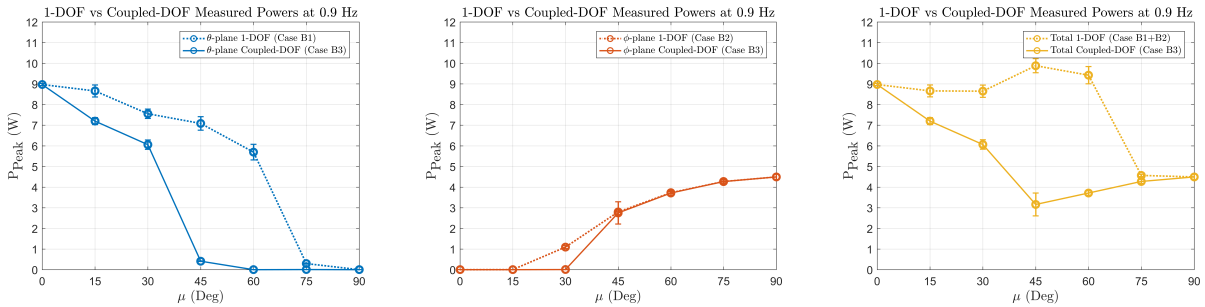

(a) θ-plane power. (b) ϕ-plane power. (c) Total power.

Fig. 11. 1-DOF vs Coupled-DOF measured steady-state peak powers at Ω = 0.9 Hz. (θ-plane = blue, ϕ-plane = red, and total = yellow).

For an example scenario, Figure 9(c) shows the maximum total power generation by utilising two 1-DOF pendulum systems (with the similar alignment in this case). The comparison of the generated total peak powers at 0.9 Hz between the example case and the coupled dynamics is shown in Figure 11(c). Consequently, for the energy harvesting application with concern to directional responses, to arrange two 1-DOF pendulum energy harvesting systems for individual perpendicular referenced axis is favourable. But, it should be highlighted that the required volume for system installation and additional weight for the optimal design are suggested to be included into the consideration.

V. Conclusions

In this paper, a novel theoretical model and a set of experimental investigations of a gimballed pendulum energy harvesting system are described. Initially, the numerical model is developed using the governing equation (Lagrange equation) with the simplified assumption that the presumed dual-perpendicular pendulum systems are created by a gimbal mechanism, and are treated as two driven planar or 1-DOF pendulum dynamic references, with geometric coupling relationships. By this method, the physical properties of the two rotating references are realistically allowed to be asymmetric. In addition, the estimated resonances (using natural frequency of linearised equation of motion) of both rotating references are possible to be theoretically and practically tuned or designed differently.

The mathematical and experimental investigations show qualitative and quantitative agreements over the tested frequency range as 1-DOF dynamic responses, in this case the heading angle (μ) is equal to 0° and 90°. For the condition that the applied excitation direction is not parallel to either rotating references, multi-directional responsiveness could be clearly achieved by the gimballed mechanism.

The coupled motions provided by the investigations show good agreement outside the estimated resonance region with comparable responded motion magnitudes when it performs as 1-DOF system, implying the coupling effect between the pendulum motions is insignificant and can be neglected. At the resonance, the dominant coupling effect is captured; however, the prediction of the pendulum motions by the mathematical model has been found to be inaccurate compared to the motions produced by the actual device test due to the simplified assumption that is made to form the equations of motion. Therefore, further theoretical research with more realistic assumption is suggested for improved understanding in this type of pendulum dynamics.

For the measured power generation, the highest power production was experimentally measured at 0.9 Hz where the largest pendulum motion and highest angular velocity occurred. This equals to linear approximation for the primary resonance. At the coupled motions mode, the responded motions respecting the two perpendicular rotating references are significantly lower due to the coupling effect. This results in the undesired lower simultaneous power production level compared to 1-DOF dynamic response at the similar excitating condition. Hence, in terms of energy conversion with the consideration of directional responses, a combination of two perpendicular 1-DOF systems may be more favourable.

Acknowledgement

This research is supported and funded by the Royal Thai Navy and the University of Southampton, United Kingdom.

Appendix A
The Dynamics of 1-DOF Driven Pendulum System

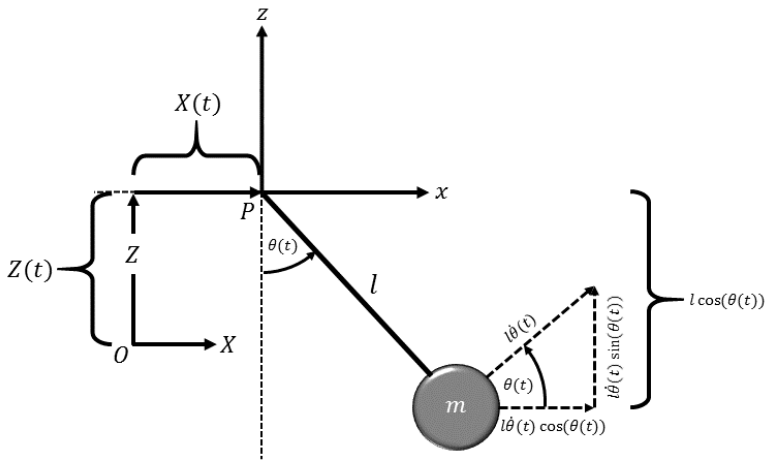

Fig. 12. Schematic diagram of a driven 1-DOF pendulum system.

Considering the schematic diagram in Figure 12, a pendulum system with a mass (m) hanging at the pivot or support point (P) at the local coordinate (Pxz) with the length (l). The support point can be disturbed and moved in horizontal (X) and vertical (Z) directions from the global reference coordinate (OXZ) which will create the resultant angle (θ) respecting the equilibrium position. So, the horizontal velocity component ($\mathbf{v}_x$) can be expressed as:

$$\mathbf{v}_x(t) = \dot{X}(t) + l\dot{\theta}(t)\cos(\theta(t)) \tag{21}$$

and the vertical velocity component ($\mathbf{v}_z$) is

$$\mathbf{v}_z(t) = \dot{Z}(t) + l\dot{\theta}(t)\sin(\theta(t)) \tag{22}$$

and, hence, the kinetic energy (T) of this pendulum system can be represented as:

$$\begin{aligned} T(t) &= \frac{1}{2}mv(t)^2 \\ &= \frac{1}{2}m\Big(\mathbf{v}_x(t) + \mathbf{v}_z(t)\Big)^2 \\ &= \frac{1}{2}m\left(\dot{X}(t) + \dot{Z}(t) + l^2\dot{\theta}(t)^2 + 2l\dot{\theta}(t)\big(\dot{X}(t)\cos(\theta(t)) + \dot{Z}(t)\sin(\theta(t))\big)\right) \end{aligned} \tag{23}$$

and, the potential energy (V) is

$$\begin{aligned} V(t) &= mgh(t) \\ &= mgl\dot{Z}(t) + mgl\Big(1 - \cos(\theta(t))\Big) \end{aligned} \tag{24}$$

and as the standard form of Lagrange equation, the governing equation, in generalised coordinate is defined as:

$$\frac{d}{dt}\left(\frac{\partial L}{\partial \dot{q}_i}\right) - \frac{\partial L}{\partial q_i} = Q_i \tag{25}$$

or, in this case, as:

$$\frac{d}{dt}\left(\frac{\partial L}{\partial \dot{\theta}}\right) - \frac{\partial L}{\partial \theta} = Q_\theta \tag{26}$$

by L is called the 'Lagrangian' which is

$$L = T - V. \tag{27}$$

Therefore, from Equations 23 and 24, the Lagrangian of the pendulum system is

$$L(t) = \frac{1}{2}m\Big(\dot{X}(t) + \dot{Z}(t) + l^2\dot{\theta}(t)^2 + 2l\dot{\theta}(t)\big(\dot{X}(t)\cos(\theta(t)) + \dot{Z}(t)\sin(\theta(t))\big)\Big) - mgl\dot{Z}(t) - mgl\Big(1 - \cos(\theta(t))\Big). \tag{28}$$

Finally, from Equation 26, the equation of motion of a driven 1-DOF pendulum system can be formulated as a second-order differential equation as:

$$ml^2\ddot{\theta}(t) + mgl\sin(\theta(t)) + ml\Big(\ddot{X}(t)\cos(\theta(t)) + \ddot{Z}(t)\sin(\theta(t))\Big) = Q_\theta \tag{29}$$

where ml^2 indicates mass moment of inertia of the pendulum (kg·m^2). $\ddot{X}$ and $\ddot{Z}$ are the horizontal and vertical accelerations (m/s^2) of the disturbance or external excitation, and Q_θ is generalised torque that represents control torque and damping component in the system. Furthermore, in case of compound pendulum system as the pendulum mass is not uniformly distributed, the equation of motion can be expressed as:

$$I\ddot{\theta}(t) + mgl\sin(\theta(t)) + ml\Big(\ddot{X}(t)\cos(\theta(t)) + \ddot{Z}(t)\sin(\theta(t))\Big) = Q_\theta \tag{30}$$

whilst I is mass moment of inertia (kg·m^2), m represents weight (kg), and l is pivot-to-CG length (m) of the pendulum system. Moreover, the undamped primary resonance can be identified as

$$\omega_n = \sqrt{\frac{mgl}{I}} \tag{31}$$

that is the undamped natural frequency of the linearised equation of motion of a simple pendulum system.

APPENDIX B
THE DYNAMICS OF 2-DOF DRIVEN SPHERICAL PENDULUM SYSTEM

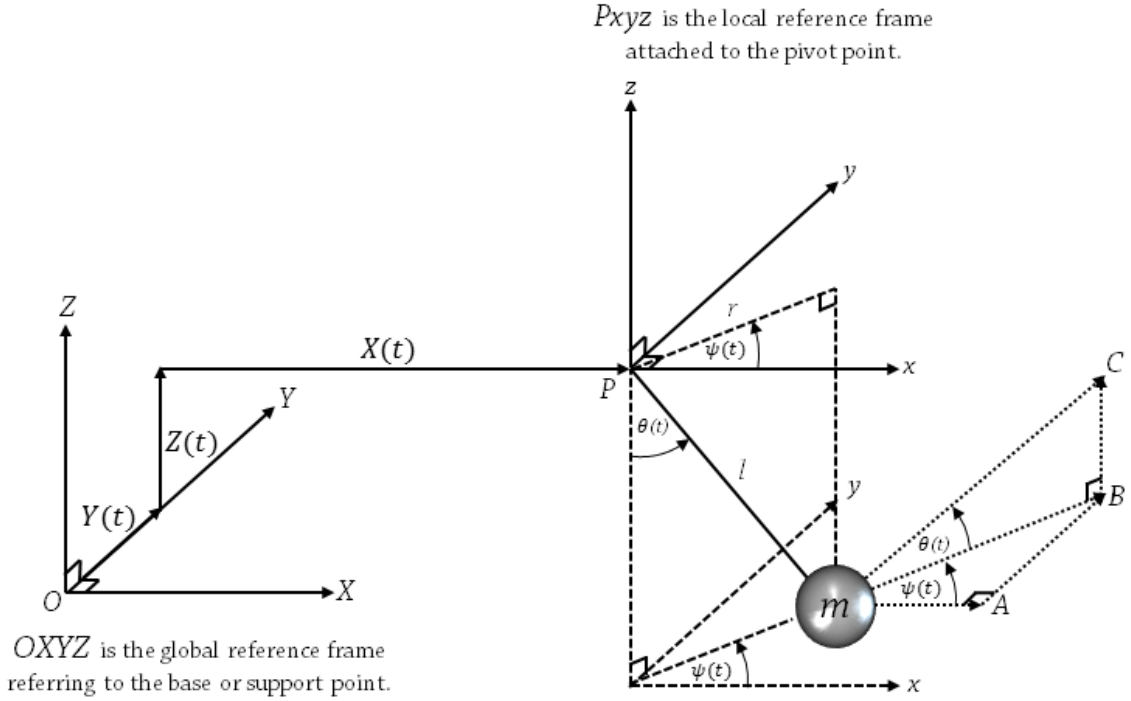

(a) Overview dynamics diagram.

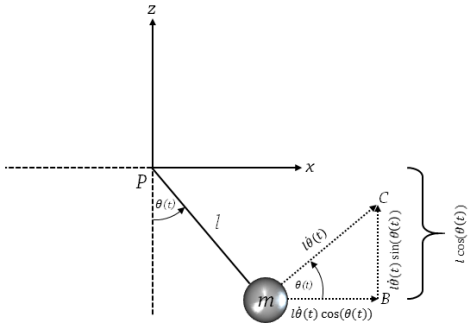

(b) xz-plane.

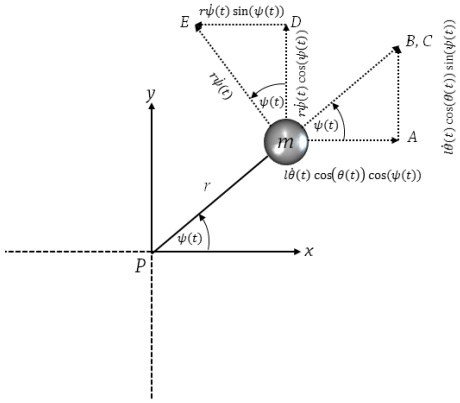

(c) xy-plane.

Fig. 13. Schematic diagram of a driven 2-DOF spherical pendulum system.

Regarding Figure 13(a), a pendulum system with mass (m) and length (l) is hanging at an unconstrained pivot point (P) which ideally allows the pendulum to complete orbital rotation around the pivot. Once, the pendulum system is disturbed from the resting position in fixed global reference coordinate ($OXYZ$) with the distances in X-, Y-, and Z-directions, the referenced angles in generalised local coordinate ($Pxyz$) are given to be the swing angle acting on vertical axis (θ) and the angle rotating around the vertical axis (ψ) of the pendulum arm that projects to the horizontal plane (xy-plane) respecting to x-axis. Consequently, from the trigonometric relations showing in Figures 13(b) and 13(c), the velocity vector components in x-, y-, and z-directions can be calculated as:

$$\mathbf{v}_x(t) = \dot{X}(t) + l\dot{\theta}(t)\cos(\theta(t))\cos(\psi(t)) - r\dot{\psi}(t)\sin(\psi(t)), \tag{32}$$

$$\mathbf{v}_y(t) = \dot{Y}(t) + l\dot{\theta}(t)\cos(\theta(t))\ \sin(\psi(t)) + r\dot{\psi}(t)\cos(\psi(t)), \tag{33}$$

$$\mathbf{v}_z(t) = \dot{Z}(t) + l\dot{\theta}(t)\ \sin(\theta(t)) \tag{34}$$

where r is the dynamic or projected pendulum length on horizontal plane (xy-plane) which is

$$r = l\sin(\theta(t)). \tag{35}$$

Therefore, the kinetic energy (T) of this pendulum system can be represented as:

$$\begin{aligned}
T(t) &= \frac{1}{2}mv(t)^2 \\
&= \frac{1}{2}m\Big(\mathbf{v}_x(t) + \mathbf{v}_y(t) + \mathbf{v}_z(t)\Big)^2 \\
&= \frac{1}{2}m\Big(\dot{X}(t)^2 + \dot{Y}(t)^2 + \dot{Z}(t)^2 - 2l\dot{X}(t)\dot{\psi}(t)\sin(\theta(t))\sin(\psi(t)) + 2l\dot{X}(t)\dot{\theta}(t)\cos(\theta(t))\cos(\psi(t)) \\
&\quad + l^2\dot{\psi}(t)^2\sin(\theta)^2 + l^2\dot{\theta}(t)^2 + 2l\dot{Y}(t)\dot{\psi}(t)\sin(\theta(t))\cos(\psi(t)) + 2l\dot{Y}(t)\dot{\theta}(t)\cos(\theta(t))\sin(\psi(t)) \\
&\quad + 2l\dot{Z}(t)\dot{\theta}(t)\sin(\theta(t))\Big)
\end{aligned} \tag{36}$$

and, from Figure 13(b), the potential energy (V) is

$$\begin{aligned}
V(t) &= mgh(t) \\
&= mgl\dot{Z}(t) + mgl\Big(1 - \cos(\theta(t))\Big).
\end{aligned} \tag{37}$$

According to the Lagrange equation, Equation 25, this pendulum system requires two governing equations for the two generalised coordinates (θ and ψ) as:

$$\frac{d}{dt}\left(\frac{\partial L}{\partial \dot{\theta}}\right) - \frac{\partial L}{\partial \theta} = Q_\theta, \tag{38}$$

$$\frac{d}{dt}\left(\frac{\partial L}{\partial \dot{\psi}}\right) - \frac{\partial L}{\partial \psi} = Q_\psi. \tag{39}$$

So, the Lagrangian of this pendulum system is

$$\begin{aligned}
L(t) &= \frac{1}{2}m\Big(\dot{X}(t)^2 + \dot{Y}(t)^2 + \dot{Z}(t)^2 - 2l\dot{X}(t)\dot{\psi}(t)\sin(\theta(t))\sin(\psi(t)) + 2l\dot{X}(t)\dot{\theta}(t)\cos(\theta(t))\cos(\psi(t)) \\
&\quad + l^2\dot{\psi}(t)^2\sin(\theta)^2 + l^2\dot{\theta}(t)^2 + 2l\dot{Y}(t)\dot{\psi}(t)\sin(\theta(t))\cos(\psi(t)) + 2l\dot{Y}(t)\dot{\theta}(t)\cos(\theta(t))\sin(\psi(t)) \\
&\quad + 2l\dot{Z}(t)\dot{\theta}(t)\sin(\theta(t))\Big) - \Big(mgl\dot{Z}(t) + mgl\Big(1 - \cos(\theta(t))\Big)\Big).
\end{aligned} \tag{40}$$

Then,

$$\begin{aligned}
\frac{d}{dt}\left(\frac{\partial L(t)}{\partial \dot{\theta}(t)}\right) &= ml^2\ddot{\theta}(t) + ml\ddot{X}(t)\cos(\theta(t))\cos(\psi(t)) - ml\dot{X}(t)\dot{\theta}(t)\sin(\theta(t))\cos(\psi(t)) - ml\dot{X}(t)\cos(\theta(t))\dot{\psi}\sin(\psi(t)) \\
&\quad + ml\ddot{Y}(t)\cos(\theta(t))\sin(\psi(t)) - ml\dot{Y}(t)\dot{\theta}(t)\sin(\theta(t))\sin(\psi(t)) + ml\dot{Y}(t)\psi(t)\cos(\theta(t))\cos(\psi(t)) \\
&\quad + ml\ddot{Z}(t)\sin(\theta(t)) + ml\dot{Z}(t)\dot{\theta}(t)\cos(\theta(t)),
\end{aligned} \tag{41}$$

$$\begin{aligned}
\frac{\partial L(t)}{\partial \theta(t)} &= ml^2\dot{\psi}(t)^2\cos(\theta(t))\sin(\theta(t)) - ml\dot{X}(t)\dot{\theta}(t)\sin(\theta(t))\cos(\psi(t)) - ml\dot{X}(t)\dot{\psi}(t)\cos(\theta(t))\sin(\psi(t)) \\
&\quad - ml\dot{Y}(t)\dot{\theta}(t)\sin(\theta(t))\sin(\psi(t)) + ml\dot{Y}(t)\dot{\psi}(t)\cos(\theta(t))\cos(\psi(t)) + ml\dot{Z}(t)\dot{\theta}(t)\cos(\theta(t)) + mgl\sin(\theta(t)),
\end{aligned} \tag{42}$$

$$\begin{aligned}
\frac{d}{dt}\left(\frac{\partial L(t)}{\partial \dot{\psi}(t)}\right) &= ml^2\ddot{\psi}(t) - ml^2\ddot{\psi}(t)\cos(\theta(t))^2 + 2ml^2\dot{\theta}(t)\dot{\psi}(t)\sin(\theta(t))\cos(\theta(t)) - ml\ddot{X}(t)\sin(\theta(t))\sin(\psi(t)) \\
&\quad - ml\dot{X}(t)\dot{\theta}(t)\cos(\theta(t))\sin(\psi(t)) - ml\dot{X}(t)\dot{\psi}(t)\sin(\theta(t))\cos(\psi(t)) + ml\ddot{Y}(t)\sin(\theta(t))\cos(\psi(t)) \\
&\quad + ml\dot{Y}(t)\dot{\theta}(t)\cos(\theta(t))\cos(\psi(t)) - ml\dot{Y}(t)\dot{\psi}(t)\sin(\theta(t))\sin(\psi(t)),
\end{aligned} \tag{43}$$

and

$$\begin{aligned}
\frac{\partial L(t)}{\partial \psi(t)} &= -ml\dot{X}(t)\dot{\theta}(t)\cos(\theta(t))\sin(\psi(t)) - ml\dot{X}(t)\dot{\psi}(t)\sin(\theta(t))\cos(\psi(t)) \\
&\quad + ml\dot{Y}(t)\dot{\theta}(t)\cos(\theta(t))\cos(\psi(t)) - ml\dot{Y}(t)\dot{\psi}(t)\sin(\theta(t))\sin(\psi(t)).
\end{aligned} \tag{44}$$

Eventually, substitute Equations 41 and 42 into Equation 38 and Equations 43 and 44 into Equation 39, two equations of motion of this driven 2-DOF spherical pendulum can be finalised as:

$$ml^2\ddot{\theta}(t) + mgl\sin(\theta(t)) - ml^2\sin(\theta(t))\cos(\theta(t))\dot{\psi}(t)^2 + ml\Big(\ddot{X}(t)\cos(\theta(t))\cos(\psi(t)) + \ddot{Y}(t)\cos(\theta(t))\sin(\psi(t)) + \ddot{Z}(t)\sin(\theta(t))\Big) = Q_\theta, \tag{45}$$

$$ml^2\sin(\theta(t))^2\ddot{\psi}(t) + 2ml^2\sin(\theta(t))\cos(\theta(t))\dot{\theta}(t)\dot{\psi}(t) - ml\sin(\theta(t))\Big(\ddot{X}(t)\sin(\psi(t)) + ml\ddot{Y}(t)\cos(\psi(t))\Big) = Q_\psi \tag{46}$$

where $\ddot{X}$, $\ddot{Y}$, and $\ddot{Z}$ are the accelerations (m/s^2) along x-, y-, and z-axes of the disturbance or external excitation. Besides, Q_θ and Q_ψ are generalised torques that representing control torques and damping components regarding referenced DOF. Likewise, the undamped primary resonance can be referred to Equation 31 in Appendix A.

REFERENCES

[1] R. A. Nelson and M. G. Olsson. The Pendulum - Rich Physics from a Simple System. *American Journal of Physics*, 54(2):112–121, feb 1986.

[2] D. J. Inman. *Engineering Vibration*. Pearson Education Limited, Essex, England, fourth edition, 2014.

[3] M. B. Dadfar and J. F. Geer. Power Series Solution to a Simple Pendulum with Oscillating Support. *SIAM Journal on Applied Mathematics*, 47(4):737–750, 1987.

[4] J. L. Trueba, J. P. Baltanás, and M. A. F. Sanjuán. A Generalized Perturbed Pendulum. *Chaos, Solitons & Fractals*, 15(5):911–924, 2003.

[5] M. Wiercigroch, A. Najdecka, and V. Vaziri. Nonlinear Dynamics of Pendulums System for Energy Harvesting. In *The 10th International Conference on Vibration Problems*, volume 139, pages 35–42. Springer Netherlands, 2011.

[6] N. A. Chaturvedi, T. Lee, M. Leok, and N. H. McClamroch. Nonlinear Dynamics of the 3D Pendulum. *Journal of Nonlinear Science*, 21(1):3–32, 2011.

[7] S. J. Roundy and J. Tola. Energy Harvester for Rotating Environments using Offset Pendulum Dynamics. *2013 Transducers and Eurosensors XXVII: The 17th International Conference on Solid-State Sensors, Actuators and Microsystems, TRANSDUCERS and EUROSENSORS 2013*, pages 689–692, 2013.

[8] E. M. Yeatman. Energy Harvesting from Motion Using Rotating and Gyroscopic Proof Masses. *Proceedings of the Institution of Mechanical Engineers, Part C: Journal of Mechanical Engineering Science*, 222(1):27–36, 2008.

[9] L. Xie, C. G. Menet, H. Ching, and R. Du. The Automatic Winding Device of a Mechanical Watch Movement and Its Application in Energy Harvesting. *Journal of Mechanical Design*, 131(7):071005, 2009.

[10] A. F. de O. Falcão. Wave Energy Utilization: A Review of the Technologies. *Renewable and Sustainable Energy Reviews*, 14(3):899–918, 2010.

[11] M. Ruellan, H. BenAhmed, B. Multon, C. Josset, A. Babarit, and A. Clement. Design Methodology for a SEAREV Wave Energy Converter. *IEEE Transactions on Energy Conversion*, 25(3):760–767, sep 2010.

[12] M. Kashiwagi, S. Nishimatsu, and K. Sakai. Wave-energy Absorption Efficiency by a Rotating Pendulum-type Electric-power Generator Installed inside a Floating Body. In *The 27th International Workshop on Water Waves and Floating Bodies*, Copenhagen, Denmark, 2012.

[13] R. Takaramoto, M. Kashiwagi, and K. Sakai. Wave Energy Absorption in Irregular Waves by a Floating Body Equipped with Interior Rotating Electric-Power Generator. *Journal of Ocean and Wind Energy*, 1(3):129–134, 2014.

[14] K. Sakai, M. Kashiwagi, and R. Takaramoto. Wave-energy Absorption by a Rotating Electric-power Generator Set inside an Asymmetric Floating Body. *Journal of the Japan Society of Naval Architects and Ocean Engineers*, 19:205–211, 2014.

[15] X. Xu. *Nonlinear Dynamics of Parametric Pendulum for Wave Energy Extraction*. PhD thesis, University of Aberdeen, 2005.

[16] K. KĘCIK. Energy Harvesting of a Pendulum Vibration Absorber. *Przegląd Elektrotechniczny*, 89(7):169–172, 2013.

[17] Y. Jia, J. Yan, K. Soga, and A. A. Seshia. Parametric Resonance for Vibration Energy Harvesting with Design Techniques to Passively Reduce the Initiation Threshold Amplitude. *Smart Materials and Structures*, 23(6):065011, jun 2014.

[18] M. Marszal, B. Witkowski, K. Jankowski, P. Perlikowski, and T. Kapitaniak. Energy Harvesting from Pendulum Oscillations. *International Journal of Non-Linear Mechanics*, 94(March):251–256, 2017.

[19] D. A. Russell. Acoustics and Vibration Animations - The Simple Pendulum Web Page. http://www.acs.psu.edu/drussell/Demos/Pendulum/Pendula.html (accessed 24 May 2018).

[20] WITT Energy Ltd. WITT Energy Website. http://www.witt-energy.com (accessed 6 May 2018).

[21] S. Crowley, R. Porter, D. J. Taunton, and P. A. Wilson. Modelling of the WITT Wave Energy Converter. *Renewable Energy*, 115:159–174, 2018.

[22] M. Hart. Proof of The Spherical Pendulum Equations of Motion - Department of Mathematics, University of Surrey Web Page, 2004.

[23] P. H. Richter, H. R. Dullin, H. Waalkens, and J. Wiersig. Spherical Pendulum, Actions, and Spin. *The Journal of Physical Chemistry*, 100(49):19124–19135, 1996.

[24] University of Southampton. Human Factors Research Unit - Laboratory Facilities. https://www.southampton.ac.uk/hfru/laboratory-facilities/index.page (accessed 13 March 2018).